CONTRACT REPORT ARBRL-CR-00455

THERMAL AND STRUCTURAL ANALYSIS OF TRAINING ROUND NOSE CAPS

Prepared by

Acurex Corporation/Aerotherm
485 Clyde Avenue
Mountain View, CA 94042

May 1981

US ARMY ARMAMENT RESEARCH AND DEVELOPMENT COMMAND
BALLISTIC RESEARCH LABORATORY
ABERDEEN PROVING GROUND, MARYLAND

Destroy this report when it is no longer needed.
Do not return it to the originator.

Secondary distribution of this report by originating or sponsoring activity is prohibited.

Additional copies of this report may be obtained from the National Technical Information Service, U.S. Department of Commerce, Springfield, Virginia 22161.

The findings in this report are not to be construed as an official Department of the Army position, unless so designated by other authorized documents.

The use of trade names or manufacturers' names in this report does not constitute indorsement of any commercial product.

UNCLASSIFIED

SECURITY CLASSIFICATION OF THIS PAGE *(When Data Entered)*

REPORT DOCUMENTATION PAGE		READ INSTRUCTIONS BEFORE COMPLETING FORM
1. REPORT NUMBER CONTRACT REPORT ARBRL-CR-00455	2. GOVT ACCESSION NO.	3. RECIPIENT'S CATALOG NUMBER
4. TITLE *(and Subtitle)* THERMAL AND STRUCTURAL ANALYSIS OF TRAINING ROUND NOSE CAPS		5. TYPE OF REPORT & PERIOD COVERED Final 6. PERFORMING ORG. REPORT NUMBER
7. AUTHOR(s) M.J. Abbett, R.P. Duiven, B. Laub, & R.A.S. Beck		8. CONTRACT OR GRANT NUMBER(s) DAAG29-76-D-0100
9. PERFORMING ORGANIZATION NAME AND ADDRESS Acurex Corporation/Aerotherm 485 Clyde Avenue Mountain View, CA 94042		10. PROGRAM ELEMENT, PROJECT, TASK AREA & WORK UNIT NUMBERS
11. CONTROLLING OFFICE NAME AND ADDRESS US Army Armament Research & Development Command US Army Ballistic Research Laboratory (DRDAR-BL) Aberdeen Proving Ground, MD 21005		12. REPORT DATE MAY 1981 13. NUMBER OF PAGES 33
14. MONITORING AGENCY NAME & ADDRESS *(if different from Controlling Office)*		15. SECURITY CLASS. *(of this report)* Unclassified 15a. DECLASSIFICATION/DOWNGRADING SCHEDULE

16. DISTRIBUTION STATEMENT *(of this Report)*

Approved for public release; distribution unlimited.

17. DISTRIBUTION STATEMENT *(of the abstract entered in Block 20, if different from Report)*

18. SUPPLEMENTARY NOTES

19. KEY WORDS *(Continue on reverse side if necessary and identify by block number)*

Aerodynamic Heating
Aerodynamic Modeling
Hypersonic Flow

20. ABSTRACT *(Continue on reverse side if necessary and identify by block number)*

This report describes the results of a brief computational study using the ABRES Shape Change Code, ASCC-79, to predict the effects of aerodynamic heating on an ablating nose cap configuration for the XM797 high velocity training round. Ablation rates and in-depth thermal response are analyzed for three flight trajectories. Recommendations are made for experimental verification of the computational modeling.

DD FORM 1 JAN 73 1473 EDITION OF 1 NOV 65 IS OBSOLETE

UNCLASSIFIED

SECURITY CLASSIFICATION OF THIS PAGE *(When Data Entered)*

TABLE OF CONTENTS

LIST OF ILLUSTRATIONS

LIST OF TABLES

I. INTRODUCTION AND OVERVIEW

A. The Problem

The XM797 projectile round is designed as a training round for the M735 high velocity projectile. As a training round, the XM797 must: (1) closely simulate the M735 trajectory for 3 km and (2) not exceed a maximum range of 8 km. To meet this second requirement, the XM797 projectile is held together with a zinc alloy nose cap which is designed to melt due to aerodynamic heating, thus breaking the projectile apart.

Firing tests of different nose cap designs and different trajectories were conducted at Yuma Proving Ground, Arizona, and Fort Greely, Alaska. Briefly summarizing the results of those tests: at Yuma, the projectiles broke-up, but not always at the expected flight times; and at Fort Greely, the projectiles broke-up much later than expected or not at all. The Yuma and Fort Greely tests differed in ambient atmospheric conditions: at Yuma the air temperature was approximately 65°F and the altitude was approximately 125 feet above sea level; at Fort Greely the air temperature was 0°F and the altitude was approximately 1750 feet above sea level. The projectiles at Yuma were assembled at ambient conditions and then placed in a temperature conditioning box to achieve initial projectile temperatures of -25°F, 70°F, and 125°F. At Fort Greely, all projectiles were assembled at ambient conditions and fired without conditioning (with a projectile initial temperature of approximately 3°F). These are the only test differences that have been identified.

The objectives of this program are to: (1) analyze the aerodynamic heating on projectile nose caps, including ablation and in-depth heat conduction effects; (2) analyze the resulting in-depth temperature distributions and material properties to predict structrual failure of the projectile nose caps; and (3) develop a plan for the experimental verification of the computational analysis.

B. Limitations and Uncertainties of the Analysis

It should be recognized that there are several areas of uncertainty in the thermal and structrual analyses. The zinc heats up and melts at the surface. The ablation and in-depth thermal analyses were done with the ABRES Shape Change Code (ASCC, Reference 1). ASCC has state of the

---

1. *Murray, A. L. and Saperstein, J. L., "User's Manual for the Updated ABRES Shape Change Code, (ASCC80)," Vol. III, Part I of the Reentry Vehicle Technology (REV-TECH) Program, FR-80-38/AS, Acurex Corporation, Mountain View, California, June 1980.*

art modeling of the flowfield, heat transfer, ablation, and in-depth conduction for projectiles, such as these training rounds. However, it has no model to account for the boundary layer-melt layer interaction, so the mass transfer rate is calculated using a convective heat transfer coefficient which is augmented for turbulent flow with an "effective sand grain roughness." This effective sand grain roughness, k_s, is determined empirically. For these calculations there were very limited resources available to estimate k_s, so there is considerable uncertainty associated with the predicted ablation rates.

The structrual calculations were obtained using the DOASIS code (Deformation Orthotropic Axisymmetric Solution of Inelastic Solids, Reference 2) to analyze the thermostructural performance of the zinc alloy nosetip for the highest priority case from the thermal analysis computations matrix (case number 1). DOASIS is a two-dimensional finite element computer code capable of determining the elastic-plastic behavior of axisymmetric solids composed of multimodulus, orthotropic materials with temperature dependent properties. Arbitrary axisymmetric thermal, pressure and body force loads can be treated. Various force and displacement boundary conditions can be selected to appropriately model various support situations. There is significant uncertainty in the mechanical properties at these evaluated temperatures; also, at these temperatures and stress-strain levels, plastic deformation is undoubtedly very important. The limited scope of this program precluded an exhaustive search for high temperature mechanical properties. Not having even estimates of plastic properties, the structrual analyses were performed using only elastic strain relations which were generated from the best data available during this short, limited study.

These are the most important limitations and uncertainties associated with this study effort. They appear significant, and they are so. However, understanding these limitations in the modeling, the results of the analyses can be used to better understand the fight data, to develop and evaluate plausible failure modes, and to identify design changes which can potentially lead to more repeatable, consistent flight performance.

C. Summary of Key Results

A cursory study of the projectile nose cap (c.f., Figure 1) leads one to immediately focus on at least two potential failure zones.

---

2. *"DOASIS, A Computer Code for the Deformation Plastic, Orthotropic, Axisymmetric (and Plane) Solution of Inelastic Solids," Air Force Materials Laboratory Report AFML-TR-75-37, October 1975.*

Should the region of the reentrant corner (A in Figure 1) be subjected to significant tensile or bending stresses, it is a likely failure point due to stress concentrations at the corner, particularly as the local temperature increases. The zinc tip is held in place by a long threaded steel bolt along the axis. The threaded contact region is indicated by $\overline{BC}$, Figure 1. Should the threads fail for any reason, or should the zinc ablate far enough to expose the air gap in front of the steel bolt (D in Figure 1), there is a high probability that a gas path will open along $\overline{BC}$, allowing the aft cavity region (E , Figure 1) to fill with hot air at stagnation point pressures (10-20 atm). This could then cause high hoop tensile stresses in the side wall, or high shear stresses in the vicinity of the second reentrant corner (F , Figure 1).

With these comments in mind, we can summarize the key results of the analyses.

1) Average predicted ablation rate and total recession are quite sensitive to uncertainties in the model of the surface energy balance (specifically, the mass removal law through the effective turbulent roughness).

2) Although there are not enough analytical results to be confident, indications are that failure occurs when the tip ablates through to the air space (D, Figure 1) in front of the steel bolt. This may be necessary for the 0.185" wall thickness tips (h = 0.185, Figure 1), in which case the failure mode is probably high hoop tensile stresses in the side wall; these would be caused by the cavity (E , Figure 1) filling with high pressure air after shear failure of the zinc to steel threads.

3) The elastic structure analyses indicate that the predominant stress loads are thermally induced, rather than mechanically (e.g., from bending due to high pressures in D , Figure 1, after burn through).

4) Additional analyses, with supporting tests, are required before failure mode and appropriate design modifications can be confidently identified.

II. ANALYSES AND DISCUSSION

A. Ablation and Heat Conduction Analyses

The matrix of cases to be considered is indicated in Table 1.

Table 1. Matrix of Cases for Ablation-Heat Conduction Analysis

Case No.	Nose Cap Configuration		Test Conditions		
	Cone Angle (deg)	Shoulder thickness (in.)	Round Temp	Atm. Temp	Trajectory
1	12.5	0.185	125°F	60°F	Yuma
2	12.5	0.185	-25°F	60°F	Yuma
3	12.5	0.185	5°F	-8°F	Ft. Greely
4	12.5	0.110	5°F	-8°F	Ft. Greely
5	12.5	0.185 (plated)	70°F	95°F	Yuma
6	12.5	0.185 (plated)	5°F	-8°F	Ft. Greely

Early in this study it became apparent that some of the uncertainty of the convective heat-mass transfer modeling could be reduced by using recent ground test data to attempt to back out the effective turbulent roughness.* The data are from zinc alloy models tested in the NASA/Ames 3-1/2 foot Hypersonic Wind Tunnel (c.f., Reference 3). The model configuration is similar to the flight article, except that the flat face is relatively thin, as indicated in the schematic below.

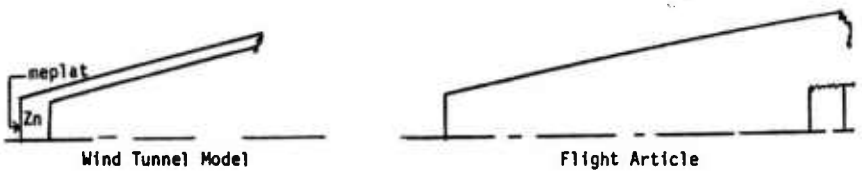

Schematic of Difference of Tip Configuration Between Wind Tunnel and Flight Article

*Since this effort was outside the scope of this study, the ablation-shape change calculation of Case 4, Table 1, was deleted and replaced with this task to calibrate the effective sand grain roughness model.

3. *Schwind, R. G., "Hypersonic Wind Tunnel Tests of Nose Cap Models Utilizing Shape Change for Range Control," Nielsen Engineering and Research, Inc., Mountain View, California, March 1979.*

During the test, melt initiation was determined visually by an onsite observer. Photographic coverage included two Hasselbald cameras using 70 mm black and white film and two Millikan motion picture cameras using 16 mm film. The framing rates were 1/30 sec for the Hasselblads and 48 and 100 frames per second for the Millikans.

For this study, we attempted to back out the effective roughness as follows. Three ASCC runs were generated for different input values of the turbulent roughness. By comparing the predicted with experimentally observed recession rate and time to burn through the meplat (c.f., preceding sketch), the effective roughness appropriate to the melting zinc could be determined empirically. The results were useful, but somewhat inconclusive, as discussed in the following paragraphs.

The steady-state ASCC calculations performed for Run No. 12 (Model 3CL) from the Ames wind tunnel test series indicated that the steady-state recession rate is directly proportional to the heat transfer coefficient on the front meplat (flat face). However, under the steady-state assumption (appropriate for a semi-infinite slab), an infinite roughness would be required to obtain the average recession rate observed during the wind tunnel test since the steady-state assumption requires that a significant fraction of the convective heating is conducted into the solid. This is demonstrated by considering the surface energy balance, illustrated below, where surface reradiation is neglected:

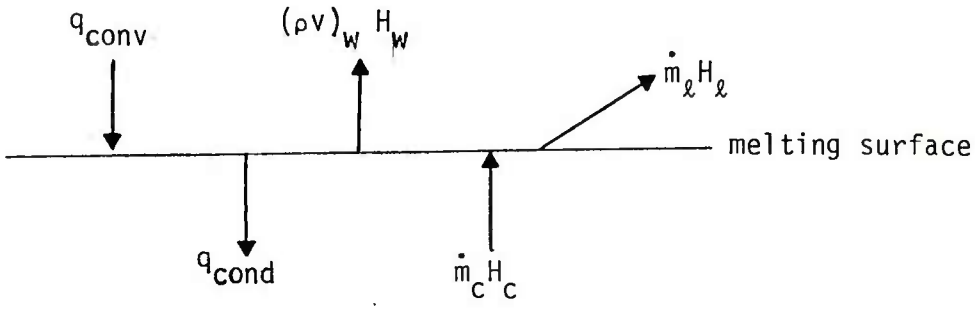

$$q_{conv} + \dot{m}_c H_c - (\rho v)_w H_w - \dot{m}_\ell H_\ell - q_{cond} = 0$$

If all diffusion coefficients are assumed equal and Prandtl and Lewis numbers are unity, the transfer-coefficient approximation gives

$$q_{conv} = \rho_e u_e C_H (H_e - H_w)$$

and

$$C_M = C_H$$

If the mass removal is only via melting, $(\rho v)_w = 0$. The steady-state ablation assumption allows the conducted energy flux to be represented by:

$$q_{cond} = \dot{m}_c (H_c - H_\infty)$$

where H is the enthalpy of the solid far from the heated surface and can be reasonably approximated by the heat of formation of the solid at the JANNAF 298°K reference state, i.e.,

$$q_{cond} = \dot{m}_c (H_c - H_\infty) \approx \dot{m}_c (H_c - \Delta H_f^0)$$

If we define

$$B' = \frac{\dot{m}_c}{\rho_e u_e C_M} = \frac{\dot{m}_\ell}{\rho_e u_e C_M}$$

$$H_c = \Delta H_f^0 + \int_{T_o}^{T_s} C_p dT \qquad \text{(enthalpy of the solid at } T_s\text{)}$$

$$H_\ell = \Delta H_f^0 + \int_{T_o}^{T_s} C_p dT + \Delta H_m \quad \text{(enthalpy of the liquid at } T_s\text{)}$$

the surface energy balance for steady-state ablation can be normalized by the mass-transfer coefficient and rewritten as:

$$H_e - H_w - B'\left[\Delta H_f^0 + \int_{T_o}^{T_s} C_p dT + \Delta H_m\right] + B'\Delta H_f^0 = 0$$

from which

$$B' = \frac{H_e - H_w}{\int_{T_o}^{T_s} C_p dT + \Delta H_m}$$

and $$\dot{s} = \frac{B'}{\rho_c}(\rho_e u_e C_H)$$

Thus, for an essentially isothermal melting material, such as the zinc alloy under consideration, the steady-state recession rate is directly proportional to the convective heat flux divided by the enthalpy of the liquid melt.

However, the steady-state approximation may be good at the onset of melting, but it becomes a progressively poorer assumption as the solid is heated in-depth. At later times lateral conduction due to heating of the sidewall combined with the finite thickness of the meplat will bring the entire meplat to near melt temperature. Under these conditions the conduction flux approaches zero and, from the surface energy balance,

$$B' = \frac{H_e - H_w}{\Delta H_m}$$

which represents the upper limit to the nondimensional mass loss rate. Even at this limiting condition the turbulent roughness required to match the average recession rate in the wind tunnel test is in the range from 50 to 100 mils.

Employing a turbulent roughness of this magnitude would represent a significant extrapolation of current roughness augmentation correlations and cannot be done with any confidence. A more significant feature observed in the high speed films of the wind tunnel tests was the relatively flat meplat surface during melting and recession. To simulate this performance with ASCC necessitates substantial laminar augmentation such that the stagnation point recession can keep pace with the corner. Reasonable shapes and recession rates were obtained with a laminar roughness of 10 mils and a turbulent roughness of 20 mils for the transient analysis of Case 1 (Table 1). Melt through to the cavity in front of the bolt was predicted at 1.38 seconds as compared to breakup at 1.18 seconds in flight. The agreement could probably be improved by increasing the assumed roughness. However, the limited scope of this study combined with the strong transient conduction effects on material performance precluded further studies to define laminar and turbulent roughness combinations that would improve the correlation of recession rate while maintaining relatively flat ablation profiles.

Using these results we conclude that 20 mils is probably a reasonable value for the effective turbulent roughness on the melt layer, and this value was used in all of the ablation calculations. There is also considerable ambiguity on the best modeling of the sidewall downstream of the region where the surface is at melt temperature, indicated by $\overline{BCD}$ in the following sketch. In the sketch, the surface is at melt

temperature along $\overline{AB}$. It is reasonable to assume that the melted zinc flows further downstream over some length, $\overline{BC}$, and that downstream of C the surface is below melt temperature and smooth (i.e., the surface is unaffected by the melt layer which is upstream). If point C is far aft of B, then the turbulent heat transfer rate along much of the sidewall should reflect the roughness augmentation, whereas if C is quite close to B, then much of the sidewall (i.e., all aft of C) should be modeled with the surface considered to be smooth.* Observations of ground test data indicate that the length $\overline{BC}$ is relatively short (c.f., Reference 3).

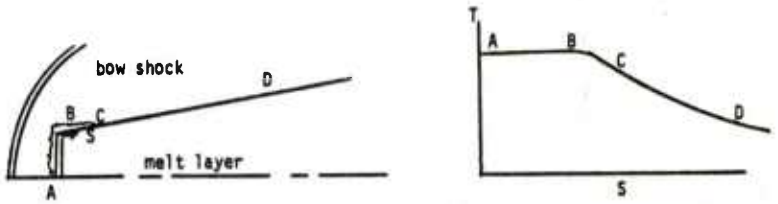

Schematic of Melt Layer and Surface Temperature Distribution

It would be nice to calculate each case using two models for the turbulent heating along $\overline{BCD}$: (1) assuming that the effective roughness due to melt layer extends the entire length of $\overline{BCD}$; and (2) assuming that wherever the surface temperature is below the melt temperature, the surface is smooth. In the latter case, the entire surface along $\overline{BCD}$ would be considered to be smooth. The limited scope of this study confines us to one full ablation-heat conduction calcualtion per flight case. Therefore, to get some feeling for the effect of these differences, we calculated Case 1 assuming that once melt is initiated on the nosetip, the entire surface, $\overline{ABCD}$, has 20 mils effective turbulent roughness. For Cases 2 and 3, we assumed that aft of the melt layer the surface is smooth, even when the flow is turbulent. It will be seen that this modeling variation has a significant effect on the predicted in-depth temperature profiles (c.f., temperature histories at the reentrant corner, A, in Figure 1) and recession rates. With this high

*Many studies of turbulent boundary layers on rough surfaces indicate that if the roughness ends at some location, the turbulent heat transfer rate rapidly (in wetted distance) approaches the appropriate smooth wall value.

conductivity material, the higher sidewall heating of Case 1 raised the in-depth temperatures enough to result in significantly higher recession rates compared to those predicted for Cases 2 and 3. We chose Case 1 to have the higher sidewall heating anticipating that the detailed structural analysis would be done for that case. The higher sidewall heating and higher in-depth temperatures are likely to result in higher thermal stresses. (However, this is not certain, since Cases 2 and 3 have higher thermal gradients in some regions.)

Most of the ablation-heat conduction study efforts were focused on Cases 1, 2, and 3. These three cases are the same except for the initial model temperature, ambient temperature, and flight trajectory. The trajectories input to ASCC correspond to those reported in Reference 4 and repeated below in Table 2 and graphed in Figure 2.

Key results of the ASCC calcualtions are presented graphically in Figures 5 through 7 as follows:

Figure 5 -- Predicted Shape Change Histories
Figure 6 -- Predicted Stagnation Point Recession Histories
Figure 7 -- Predicted Temperature Histories at Stagnation Point and Reentrant Corner

---

4. *Sturek, W. B. and Mylin, D. C., "Preliminary Computations of Aerodynamic Heating for XM797 Nose Cap Configurations," Ballistic Research Laboratory, Aberdeen Proving Ground, Maryland, BRL Memorandum Report in preparation.*

Table 2. Trajectory Data

Time (sec)	Case 1 Velocity (fps)	Case 2 Velocity (fps)	Case 3 Velocity (fps)
0.000	5259.00	4905.00	4986.50
0.200	5184.00	4813.00	4873.70
0.400	5082.00	4718.00	4766.00
0.600	4941.00	4610.00	4661.99
0.800	4793.00	4505.00	4445.56
1.000	4636.00	4390.00	4329.42
1.200	4446.00	4275.00	4205.31
1.400	4249.00	4154.00	4079.98
1.600	4035.00	4019.00	3954.81
1.800	3839.00	3891.00	3833.85
2.000	3629.00	3773.00	3719.58
2.200	3406.00	3638.00	3611.57
2.400	3169.00	3497.00	3510.26
2.600	2946.00	3343.00	3415.31
2.800	2723.00	3203.00	3326.08
3.000	2510.00	3054.00	3242.05

First, by reference to Figures 5, 6, and 7, it is clear that predicted stagnation point recession and recession rate are quite sensitive to the side wall heat transfer modeling. Cases 2 and 3 had nominally the same trajectories and quite similar predicted shape change and stagnation point recession histories. Case 1, with approximately 5 to 7 percent higher velocity during the first second, has a much higher recession rate, receding a total of 0.77" in the first 1.2 sec compared to 0.43 and 0.48 sec for Cases 2 and 3 respectively. Such large differences cannot be mostly attributed to the trajectory differences. An examination of the in-depth temperature profiles indicates that the higher sidewall heat transfer modeled in Case 1 rapidly leads to significantly higher in-depth temperatures along the axis. Thus, less heat is conducted away from the surface and higher stagnation region recesion rates result.

Second, an examination of the temperature histories at the reentrant corner (A in Figure 1) indicates that this region probably does not reach melt temperature. However, the rate at which the predicted temperature increases at A is sensitive to the assumed side wall heat transfer model.

Third, we see that the prediction for Case 1 indicates burn through at about 1.38 sec, whereas neither the Case 2 and Case 3 predictions indicate burn through by three seconds of flight.

Before discussing the structural calculations for Case 1, it is useful to discuss expected trends based on the ablation-thermal analyses. First we expect Case 1 to recede faster than Case 2. Both rounds were fired at the same atmospheric conditions. Case 1 had a higher initial velocity and higher initial projectile temperature, both of which would cause higher ablation rates and earlier burn through.

Comparing Cases 2 and 3, the lower ambient and model temperatures of Case 3 would both tend to decrease the recession rate. The slightly higher velocities during the first 0.7 sec would tend to give somewhat higher recession rate, but these are later offset by the correspondingly slightly lower velocities after 0.8 sec. Examination of the shape change and stagnation point recession plots, Figures 5b, 5c, and 6 indicate that predicted shape change and recession are almost identical for these two rounds.

The actual flight experience is as follows. Case 1 broke up after 1.18 sec, which is just before the 1.38 sec predicted for burn through. Case 2 broke up after 2.25 sec, and the flight article for Case 3 did not break up. If the side wall heating model used in the Case 1 prediction had been used in Cases 2 and 3, the prediction would have indicated burn through slightly later than for Case 1.

Before discussing the structrual analyses, we briefly summarize the results of the heat transfer-heat conduction calculations for Cases 5 and 6. These projectiles were plated with a thin steel plate which would not melt under flight conditions. Since the ASCC code does not account for the heat of fusion due to in-depth melting.* Cases 5 and 6 were each treated as one of the two limits, infinite and zero heat of fusion respectively. The calculated temperature histories at the stagnation point and the reentrant corner are shown in Figures 7d and 7e, respectively. In each case the maximum temperature reached at the reentrant corner is about 900°R, and this is reached after 3 sec of flight. There will be no further discussion of these cases in this report.

B. Structural Analyses

As noted earlier, thermal-structrual analyses were made using the DOASIS code. These analyses include part of the steel backing as illustrated in Figure 8, which shows the finite element grid. Four thermal-structural solutions were generated, all for Case 1. The calculations differed in two ways.

---

*The heat of fusion is properly accounted for in the surface energy balance calculation when melting occurs only at the surface, as in Cases 1, 2, and 3.

Two calculations assumed that the tip had burned through, exposing the cavity (D), Figure 1, to high pressure stagnation air. These calculations were to test the hypothesis that this high pressure could cause large bending stresses in the vicinity of the reentrant corner (A Figure 1). The two calculations differed in the modeling of the material properties in gap regions, as discussed below.

The other two calculations had the same variation in gap region modeling, but they were for times just prior to burn through. Thus, the cavity ((D), Figure 1) was not pressurized.

Gap modeling in the first two calculations treated the gap elements as multi-modulus materials, having stiff compressive properties and very flexible tensile properties. With this approximation the DOASIS code uses a multi-modulus theory which employs stress weighted coefficients for the cross-compliances. The resulting displacement and stress fields were unrealistic, so two more calculations were generated in which the gaps were modeled as a mixed-modulus material. In this case, those areas which are in hydrostatic tension use the tensile (flexible) modulus while those areas in hydrostatic compression use the compressive (stiff) modulus. The resulting displacement and stress solutions are much more consistent and believeable.*

The zinc and steel were both treated as isotropic temperature dependent materials. A summary of the material properties used in the analysis is presented in Table 3.

The finite element nodal grid is shown in Figure 6. The boundary conditions consisted of holding the back portion of the steel against axial movement ($\Delta Z = 0$) and also applying the symmetry condition of $\Delta R = 0$ along the centerline of the bolt.

---

*Keep in mind that these predictions assume completely elastic behavior. An elastic-plastic analysis was not done because of the lack of high temperature plastic properties.

Table 3. Material Properties for Structural Calculations

Temp (°F)	Modulus 10^6 (psi)	Poisson's Ratio	10^6 (in./in./^{0}F)
Zinc			
70	13.10	0.3	15.20
200	12.71	0.3	15.20
300	11.92	0.3	15.20
400	10.61	0.3	15.20
500	8.52	0.3	15.20
600	6.03	0.3	15.20
700	3.41	0.3	15.20
800	0.01	0.3	15.20
4130 Steel			
70	30.0	0.3	6.3
400	28.5	0.3	6.3
600	27.3	0.3	6.3
800	24.9	0.3	6.3
1000	21.0	0.3	6.3

The ablated shape, internal thermal field, and external pressure distribution were obtained directly from the results of the ASCC solution. An angular velocity of 30 revolutions/second was applied as a body force. Also, an initial bolt preload of 800 lb, corresponding to a torque of 30 in-lb, was applied along the thread elements.

Two different loading conditions were examined: with and without stagnation pressure in the small cavity ahead of the end of the bolt. It was anticipated that the addition of pressure in this cavity might radially open the threads, bend the forward portion of the zinc nosetip outward and produce large bending stresses across the shell near the reentrant corner.

However, the displacement and stress fields in both cases were quite similar, quantitatively as well as qualitatively. Additional pressure in the cavity did produce slightly more radial expansion of the

tip of the nose, but this effect was small and did not propagate back past the thread region. In these cases, the stress field is dominated by thermally induced stresses.

The results of both analyses do point to the possible failure modes. The first, and most likely, is thread shear failure of the zinc threads. The differential axial growth along the threads, due to the differential thermal expansion of the zinc and steel, produces higher shear stresses in the region. The maximum predicted shear stress in the zinc just radially outboard of the threads was found to be 29,600 psi. The average stress across this region was 23,038 psi. Coupled with the very low shear strength existing at the average thread temperature of 660°F, thread shear failure is very likely.

Another area of interest was the inside edge of the 0.185 inch side wall. A high tensile hoop stress field is predicted to occur along this wall. The maximum stress value is 51,720 psi which is well in excess of the strength of the zinc. However, it is recognized that most (if not all) of this tensile field is thermally induced and is balanced by hoop compressive stresses through the remainder of the wall. Furthermore, plastic analysis of this region would reduce the hoop tensile stress field, which was determined from an elastic procedure. Although failure could possibly be initiated here, the mode is not thought to be as critical as the thread shear mode.

One other area of interest was right at the reentrant corner. A maximum shear stress of 12,100 psi was calculated there. The element temperature is 690°F and the shear strength of zinc, is sufficiently reduced at this temperature to possibly lead to failure of the corner in shear. Again, plastic redistribution would tend to reduce this stress.

In conclusion, the most probable failure mode identified by the thermostructural analysis which was performed is thread shear failure of the zinc threads, due to the shear loads induced across the threads by the differential thermal expansion of the steel and the zinc. Greater confidence in identifying the most probable failure mode can be realized by performing additional transient shape change and thermostructural calculations and from experimental data as discussed in the following subsection and section 3.

C. Discussion of Ground and Flight Test Considerations

There are at least four ways in which data from ground tests can contribute to the development of the training round design.

1) Parametrically screen candidate configurations.
2) Identify the failure mode under simulated flight conditions.
3) Calibrate models used in analytical studies.
4) Verify the adequacy of a specific design.

To fulfill objectives 1), 2), and 4), it is necessary to achieve good simulation of heat and mass transfer rates experienced in flight. Though this is also desirable for 3), it is not absolutely necessary.

Parametrically screening candidate design options and variations is particularly suitable when there is little or no uncertainty about the failure mode. However, when the failure mode is uncertain, as in the present circumstances, there is a high risk that such an approach will not result in varying the most appropriate parameters; or, they may be varied in a far from optimum matrix.

The most useful data would be obtained from tests which are designed to identify the failure mode(s). Unfortunately, such tests are relatively expensive, in terms of both cost and schedule. Such a test series would involve instrumenting models with strain gauges, and it would include detailed photographic coverage.

Analytic studies are quite useful to guide the design effort, including considering various parametric trade-offs. The usefulness of the analysis depends on its reliability. For example, as discussed previously, there is considerable uncertainty on the heat and mass transfer modeling use in these calculations. That uncertainty could be reduced significantly if there were available adequate data to calibrate the effective roughness model used in the ASCC calculations.

Finally, prior to final flight test verification, design verification tests in ground facilities are very useful to minimize the uncertainty associated with final design. If some design inadequacies remain, ground tests are more likely to yield information which will help rectify the inadequacy.

There are many parameters which are important to simulate in the ground test. The most important are stream total enthalpy, model stagnation point pressure, and model size (to ensure correct thermostructural scaling). Wind tunnels are inadequate because the total enthalpy is too low. Therefore, the low resulting heat and mass transfer rates will lead to inadequate simulation of the in-depth temperature profile and thermal stress history.

Probably the best simulation of flight conditions can be achieved in plasma arc type test facilities, though there are problems with arcs as well. Generally, arc plasma facilities are designed to yield flows with high thermal energy. It is difficult to find a facility which simultaneously matches the enthalpy and stagnation point pressure needed for these tests. For example, the 50 MW facility at WPAFB and the HEAT

facility at AEDC can both achieve the needed pressures, but the enthalpies would be much too high and the allowable model size is probably a little too small.

A cursory review of existing arc test facilities indicates that the AVCO 10 MW facility is probably the most suitable for this test program (c.f., Reference 5). In that facility one can closely duplicate the desired total enthalpy (~500 Btu/lb) and stagnation point pressures (10 to 25 atm) on a full scale model. However, there are two definite shortcomings, one of which may preclude the possibility of adequately simulating the thermostructral response, and perhaps even the transient recession rate. The least serious shortcoming is that the arc facility utilizes carbon cathodes which themselves ablate, contaminating the stream. Reported contamination levels are 1 to 5 percent by mass. These particles can affect the overall boundary layer-surface ablation interaction, again modifying the ablation rate. However, this shortcoming is not considered so severe as to preclude obtaining useful data from tests in that facility.

The second shortcoming is more serious, at least for this program. As discussed in more detail in Reference 5, the model bow shock interacts with the jet constant pressure boundary, reulting in repeated regions of low and high heat flux along the model side wall. These heat flux variations are large enough to cause zones of spallation along the side walls of ablative materials, as shown in Figure 7, which is reproduced from Reference 5. Such nonuniform interaction heating will undoubtedly modify the in-depth temperature and stress fields, and it is very possible that such a test is invalid from a thermostructural point of view.

However, this does not mean that such tests are useless. Using sidewall heat flux distributions obtained experimentally, tests in the AVCO 10 MW facility can be used to calibrate shape-change modeling. In addition, they can be used to evaluate the reliability of a forced failure, such as by pressurizing the internal cavity as discussed above.

III. CONCLUDING REMARKS

It is clear from this analysis that the failure mode(s) of the flight article is uncertain. There is a high probability that there is thread shear failure along the interface between the zinc tip and the steel bolt along the axis. When the recession rate is high enough to

---

5. *Avco staff, "Avco Hyperthermal Simulation Capabilities," Avco Systems Division, AVSD-0457-70-CA, Wilmington, Massachussetts, 14 Sept. 1970.*

expose the steel bolt, it is likely that high pressure will enter the cavity (Ⓔ, Figure 1). This would probably cause higher shear stresses in the vicinity of the reentrant corner(A , Figure 1).

Since the zinc threads are approximately within 100°F of the melt temperature, it is possible for this "soft" material to form a gas seal, thus precluding pressurization of cavity Ⓔ. One can also postulate that the rear cavity, Ⓔ, would be pressurized immediately upon exposure of the cavity in front of the bolt, Ⓓ, i.e., upon melt-through of the nosetip. Therefore, it is not clear that the performance in this region is repeatable. This is consistent with the flight performance which also demonstrated nonrepeatability (e.g., Case 2 versus Case 3).

For the cases which were analyzed thermostructrually in this study, thermally induced stresses were quite high. Considering the relatively short flight interval in which failure is desired to occur, it is probably desirable to force failure through some other mechanism than thermally induced stresses. Also, it is probably important to ensure that, once melting has begun, the side wall boundary layer is not transitional. It may well be that adequate repeatability of the stagnation region recession rate depends on ensuring that the boundary layer on the side wall is turbulent and that the surface there is preroughened in a controlled manner.

This study has identified several potential failure modes for the training round, but existing uncertainties in the data and this limited study preclude resolution of the anomalous flight results. Sufficient insight into materials performance has been gained through this study to suggest that some well-designed ground tests accompained by complementary analyses can define the major failure models, with some certainty, thus leading to a reliable design.

REFERENCES

1. Murray, A.L. and Saperstein, J.L., "User's Manual for the Updated ABRES Shape Change Code, (ASCC80)," Vol, III, Part I of the Reentry Vehicle Technology (REV-TECH) Program, FR-80-38/AS, Acurex Corporation, Mountain View, California, June 1980.

2. "DOASIS, A Computer Code for the Deformation Plastic, Orthotropic, Axisymmetric (and Plane) Solution of Inelastic Solids", Air Force Materials Laboratory Report AFML-TR-75-37, October 1975.

3. Schwind, R.G., "Hypersonic Wind Tunnel Tests of Nose Cap Models Utilizing Shape Change for Range Control", Nielsen Engineering and Research, Inc., Mountain View, California, March 1979.

4. Sturek, W.B. and Mylin, D.C., "Preliminary Computations of Aerodynamic Heating for XM797 Nose Cap Configurations", U.S. Army Ballistic Research Laboratory, ARRADCOM, IMR 684, June 1980.

5. Avco staff, "Avco Hyperthermal Simulation Capabilities", Avco Systems Division, AVSD-0457-70-CA, Wilmington, Massachusetts, 14 September 1970.

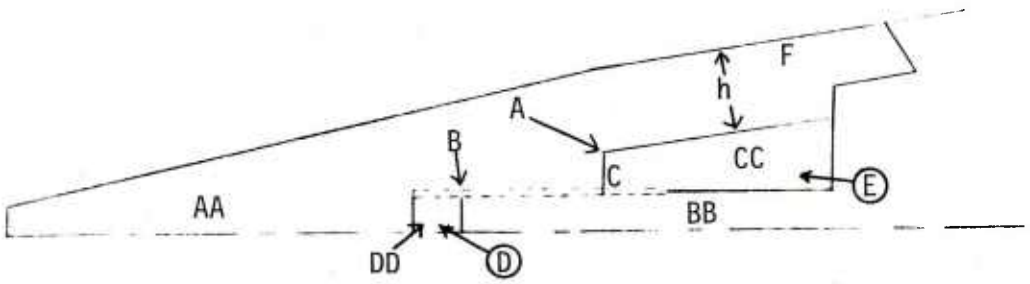

AA - ZINC
BB - STEEL
CC - AIR
DD - AIR

Figure 1. Schematic of Training Round Tip and Substructure

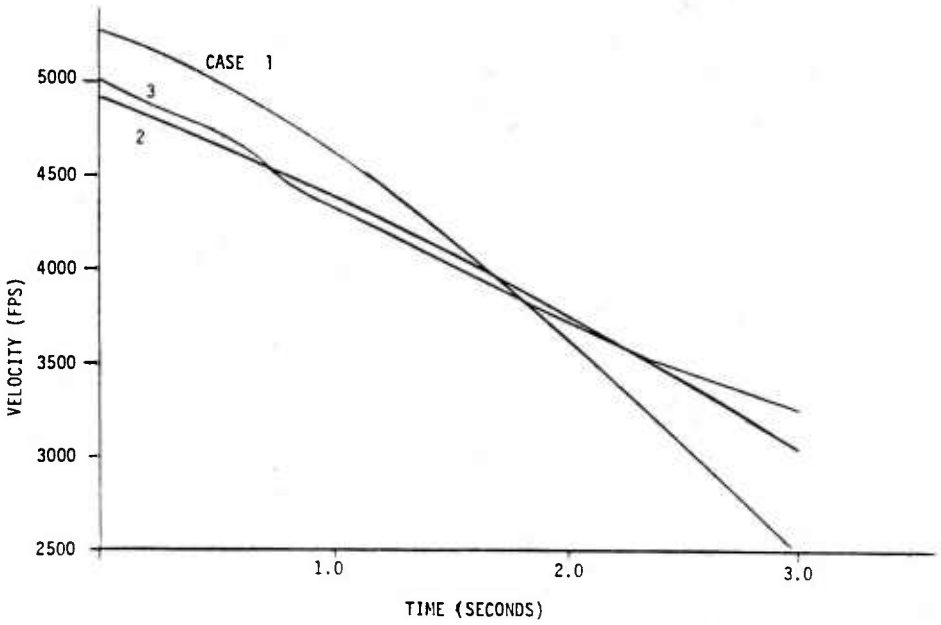

Figure 2. Trajectory Histories--Cases 1, 2, and 3

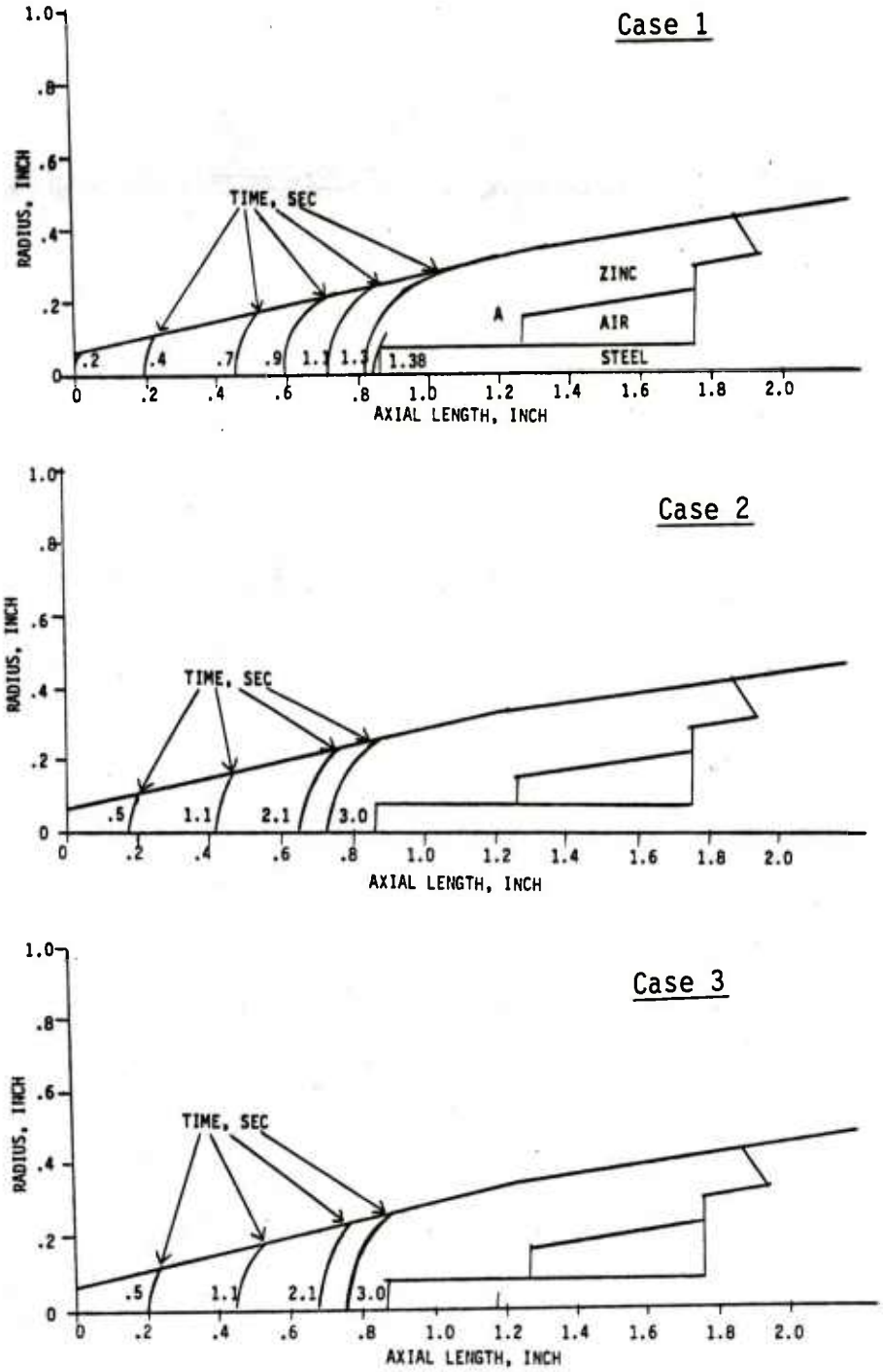

Figure 3. Predicted Shape Change Histories

a. Case 1

b. Case 2

c. Case 3

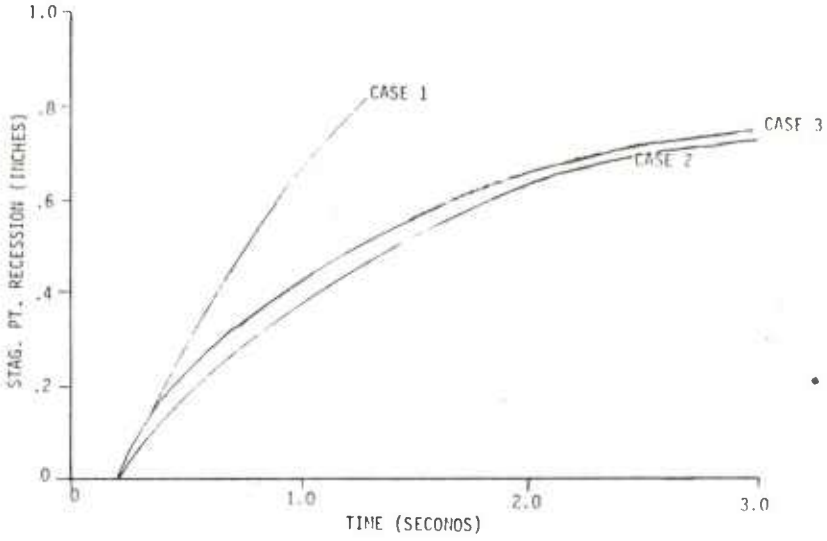

Figure 4. Predicted Stagnation Point Recession

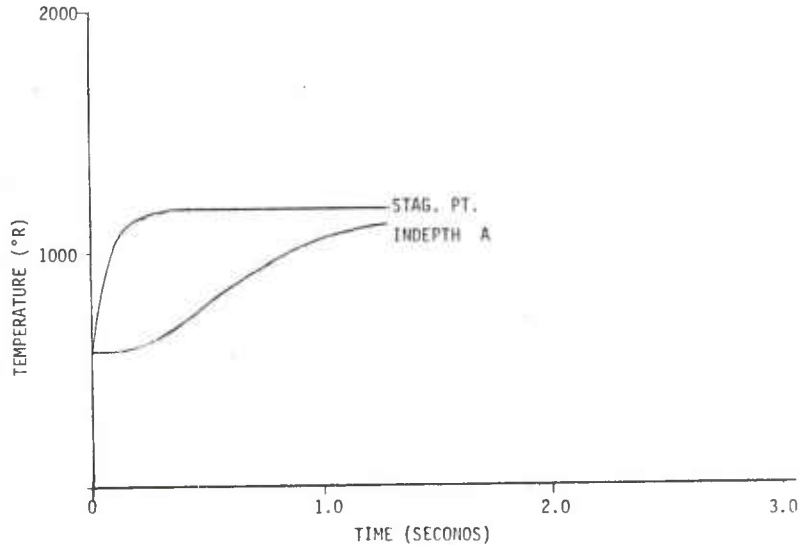

Figure 5. Temperature Histories at Stagnation Point and Reentrant Corner

a. Case 1

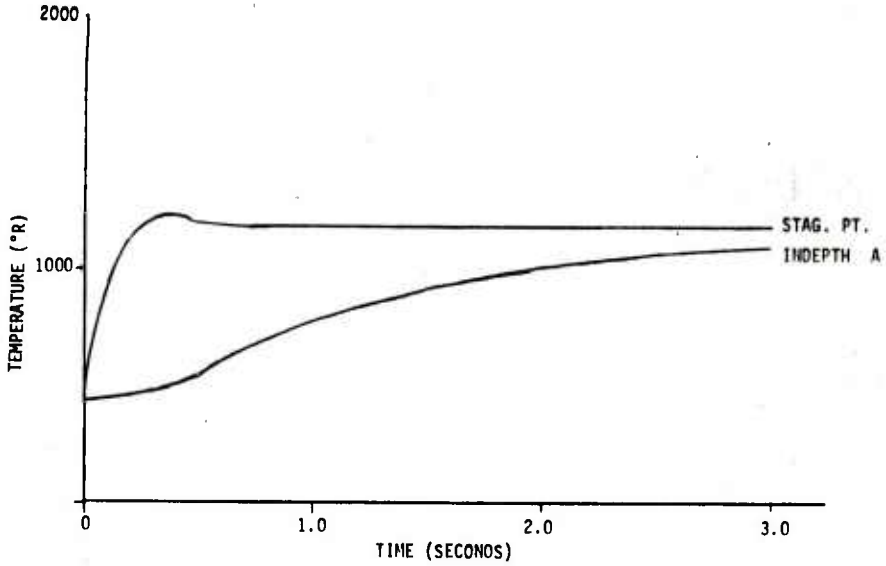

Figure 5. Continued

b. Case 2

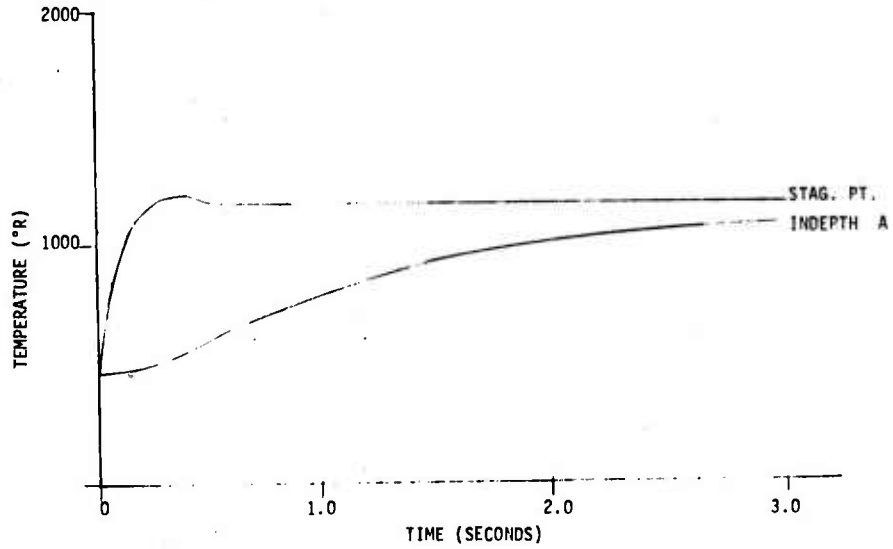

Figure 5. Continued

c. Case 3

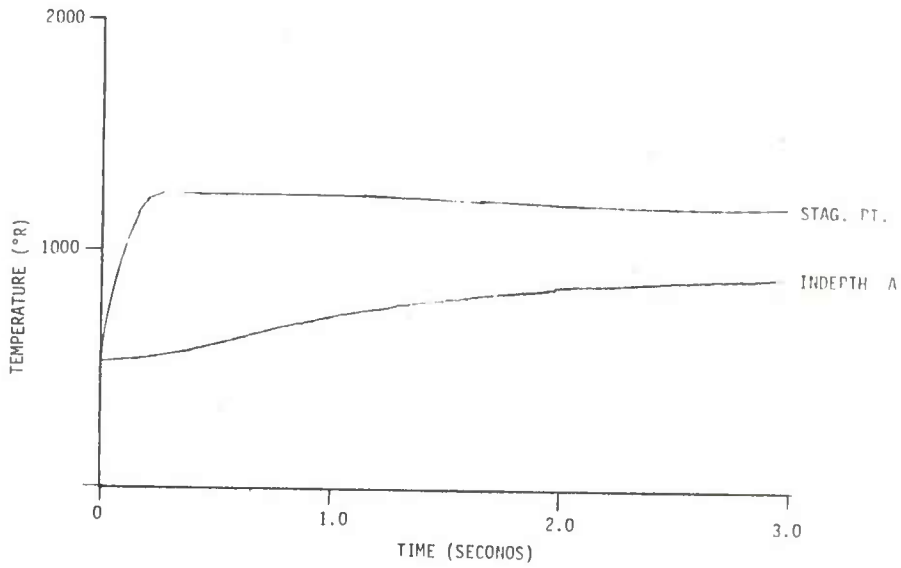

Figure 5. Continued

d. Case 5

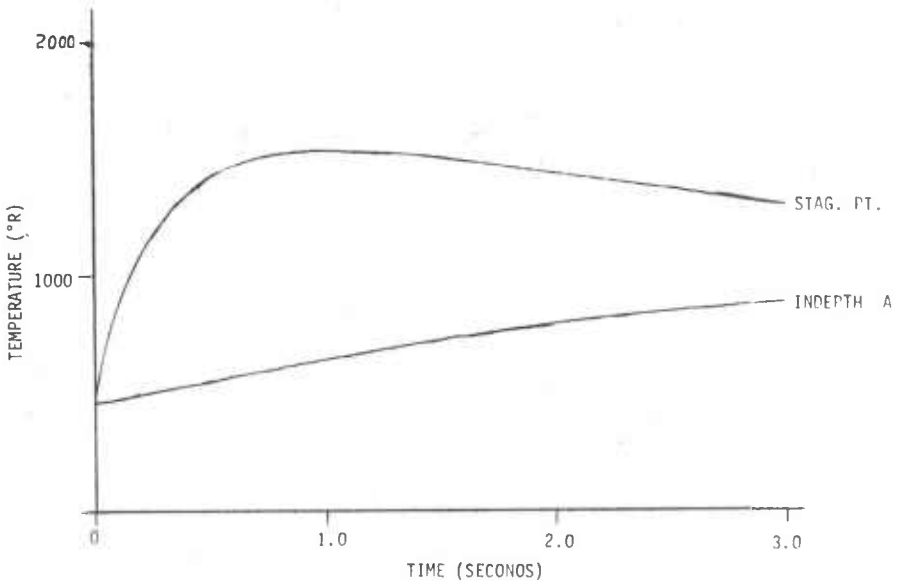

Figure 5. Continued

e. Case 6

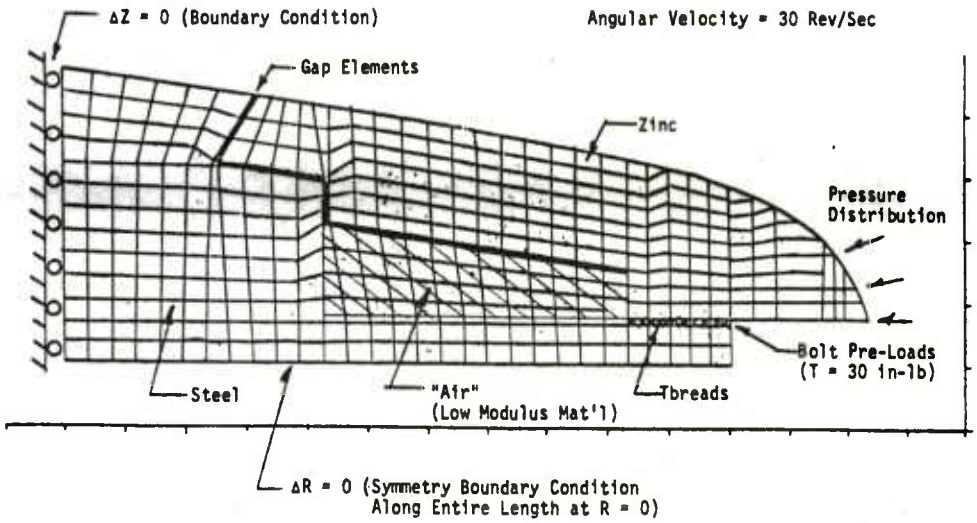

Figure 6. Finite Element Grid

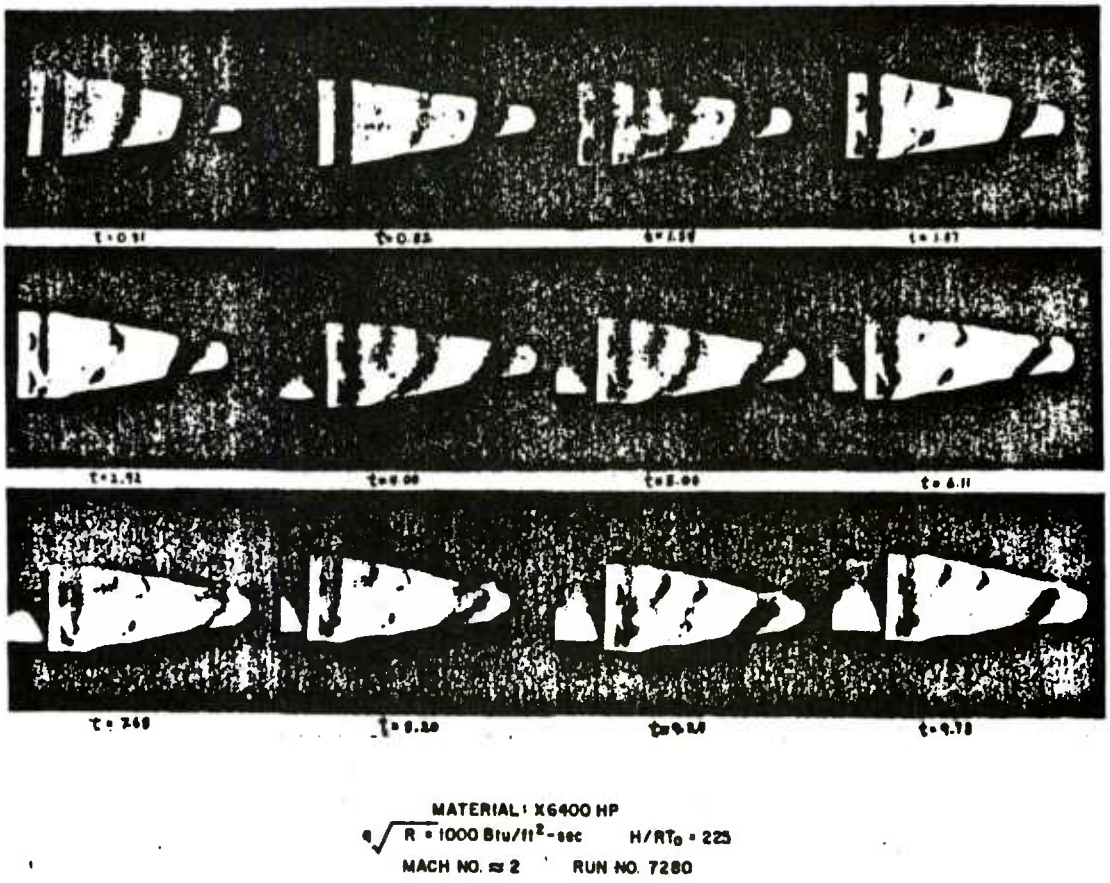

Figure 7. Ten-Megawatt Arc Tip Test Phenomena (Reproduced from Reference 5)

DISTRIBUTION LIST

No. of Copies	Organization
12	Commander Defense Technical Info Center ATTN: DDC-DDA Cameron Station Alexandria, VA 22314
1	Commander US Army Materiel Development and Readiness Command ATTN: DRCDMD-ST 5001 Eisenhower Avenue Alexandria, VA 22333
8	Commander US Army Armament Research and Development Command ATTN: DRDAR-TSS (2 cys) DRDAR-LCA-F Mr. D. Mertz Mr. E. Falkowski Mr. A. Loeb Mr. R. Kline Mr. S. Kahn Mr. S. Wasserman Dover, NJ 07801
1	Commander US Army Armament Materiel Readiness Command ATTN: DRSAR-LEP-L, Tech Lib Rock Island, IL 61299
1	Director US Army Armament Research and Development Command ATTN: DRDAR-LCB-TL Watervliet, NY 12189
1	Commander US Army Aviation Research and Development Command ATTN: DRSAV-E P. O. Box 209 St. Louis, MO 61366
1	Director US Army Air Mobility Research and Development Laboratory Ames Research Center Moffett Field, CA 94035
1	Commander US Army Communications Research and Development Command ATTN: DRDCO-PPA-SA Fort Monmouth, NJ 07703
1	Commander US Army Electronics Research and Development Command Technical Support Activity ATTN: DELSD-L Fort Monmouth, NJ 07703
3	Commander US Army Missile Command ATTN: DRSMI-R DRSMI-RDK Mr. R. Deep Mr. R. Becht Redstone Arsenal, AL 35809
1	Commander US Army Missile Command ATTN: DRSMI-YDL Redstone Arsenal, AL 35809
1	Commander US Army Tank Automotive Research and Development Command ATTN: DRDTA-UL Warren, MI 48090

DISTRIBUTION LIST

No. of Copies	Organization
1	Director US Army TRADOC Systems Analysis Activity ATTN: ATAA-SL, Tech Lib White Sands Missile Range, NM 88002
1	Commander US Army Research Office P. O. Box 12211 Research Triangle Park NC 27709
1	Commander US Naval Air Systems Command ATTN: AIR-604 Washington, D. C. 20360
2	Commander David W. Taylor Naval Ship Research and Development Center ATTN: Dr. S. de los Santos Mr. Stanley Gottlieb Bethesda, Maryland 20084
4	Commander US Naval Surface Weapons Center ATTN: Dr. T. Clare, Code DK20 Dr. P. Daniels Mr. D. A. Jones III Mr. L. Mason Dahlgren, VA 22448
4	Commander US Naval Surface Weapons Center ATTN: Code 312 Mr. R. Voisinet Mr. R. Driftmeyer Mr. J. Knott Mr. R. Schlie Silver Spring, MD 20910
1	Commander Naval Weapons Center ATTN: Code 3431, Tech Lib China Lake, CA 93555
1	Director NASA Langley Research Center ATTN: NS-185, Tech Lib Langley Station Hampton, VA 23365
4	Director NASA Ames Research Center ATTN: MS-202A-14, Dr. P.Kutler MS-202-1, Dr. T.Pullinam MS-227-8, Dr. L. Schiff MS-202, Tech Lib Moffett Field, CA 94035
1	ARO, Inc. von Karman Gas Dynamics Facility ATTN: Dr. John C. Adams, Jr. Aerodynamics Division Projects Branch Arnold AFS, TN 37389
4	Acurex Corporation/Aerotherm ATTN: M. J. Abbett R. P. Duiven B. Laub R.A.S. Beck 485 Clyde Avenue Mountain View, CA 94042
1	Nielsen Engineering & Research, Inc. ATTN: Dr. S. Stahara 510 Clyde Avenue Mountain View, CA 94043
1	Sandia Laboratories ATTN: Division No. 1331, Mr. H. R. Vaughn P. O. Box 580 Albuquerque, NM 87115

DISTRIBUTION LIST

No. of Copies	Organization
2	Massachusetts Institute of Technology ATTN: Prof. E. Covert Prof. C. Haldeman 77 Massachusetts Avenue Cambridge, MA 02139
1	Stanford University Department of Aeronautics and Astronautics ATTN: Prof. J. Steger Stanford, CA 94035
1	University of California, Davis Department of Mechanical Engineering ATTN: Prof. H.A. Dwyer Davis, CA 95616
1	University of Colorado Department of Aerospace Engineering ATTN: Prof. G. Inger Boulder, CO 80309
1	University of Delaware Mechanical and Aerospace Engineering Department ATTN: Dr. J. E. Danberg Newark, DE 19711

Aberdeen Proving Ground

Director, USAMSAA
ATTN: DRXSY-D
DRXSY-MP, H. Cohen

Commander, USATECOM
ATTN: DRSTE-TO-F

Dir, USACSL, Bldg. E3516
ATTN: DRDAR-CLB-PA
Mr. M. Miller

USER EVALUATION OF REPORT

Please take a few minutes to answer the questions below; tear out this sheet, fold as indicated, staple or tape closed, and place in the mail. Your comments will provide us with information for improving future reports.

1. BRL Report Number _____

2. Does this report satisfy a need? (Comment on purpose, related project, or other area of interest for which report will be used.)

_____

_____

_____

3. How, specifically, is the report being used? (Information source, design data or procedure, management procedure, source of ideas, etc.) _____

_____

_____

4. Has the information in this report led to any quantitative savings as far as man-hours/contract dollars saved, operating costs avoided, efficiencies achieved, etc.? If so, please elaborate.

_____

_____

5. General Comments (Indicate what you think should be changed to make this report and future reports of this type more responsive to your needs, more usable, improve readability, etc.) _____

_____

_____

_____

6. If you would like to be contacted by the personnel who prepared this report to raise specific questions or discuss the topic, please fill in the following information.

Name: _____

Telephone Number: _____

Organization Address: _____

_____

_____